THE ASTROPHYSICAL JOURNAL, 224:614–624, 1978 September 1

X-RAY TRANSFER IN BINARY SYSTEMS: A MONTE CARLO STUDY*

P. HERTZ, P. C. JOSS,† AND S. RAPPAPORT†
Department of Physics and Center for Space Research, Massachusetts Institute of Technology
Received 1978 January 4; accepted 1978 March 10

ABSTRACT

We have devised simple models of X-ray binary systems surrounded by gas clouds and have performed Monte Carlo simulations of the resultant orbital X-ray light curves. Occultation of the X-radiation by the companion star, as well as Compton scattering and photoelectric absorption within the gas cloud that surrounds the system, is taken into account. The cloud densities are assumed to be symmetric with respect to the companion star and hence distinctly asymmetric with respect to the X-ray star.

We discuss the applicability of our results to models for specific binary X-ray sources. In particular, we draw (or confirm) the following conclusions: (1) Broad geometrical eclipses probably cannot be obscured unless the cloud has a large Compton-scattering optical depth ($\tau_e \gtrsim 5$) and a scale size that is large compared to the size of the binary orbit. (2) The production of iron X-ray emission lines by fluorescence, during transfer of X-radiation through a cloud, leads to X-ray absorption features of comparable magnitude. Because absorption and emission features have not yet been observed simultaneously in galactic X-ray sources, the actual mechanism for iron-line production must be more complex and involve collisional ionization. (3) A strong and variable stellar wind can approximately replicate the variable "choking" behavior and nonzero eclipse intensity observed in Cen X-3 (Schreier *et al.*). (4) A "cocoon" model for Cyg X-3, proposed by Milgrom, reproduces many of the essential observational properties of this source. The fundamental requirements of such a model are that the cloud have a scale size that is large compared to the size of the binary orbit, have a high degree of ionization (except perhaps in the shadow of the companion star), and have $\tau_e \gtrsim 2$.

Subject headings: stars: eclipsing binaries — X-rays: binaries — X-rays: spectra

I. INTRODUCTION

The orbital X-ray light curves of binary X-ray sources provide information about the parameters of the X-ray and companion stars and the character of mass loss and mass exchange in the binary systems. Pioneering efforts to understand the physics of the transfer of X-radiation through a surrounding gas cloud have been carried out by Tarter, Tucker, and Salpeter (1969), Tarter and Salpeter (1969), Pringle (1973), Buff and McCray (1974*a*, *b*), Hatchett, Buff, and McCray (1976), and Hatchett and McCray (1977). More specialized attempts to interpret the X-ray light curves have been made in the case of Cyg X-3 (Davidsen and Ostriker 1974; Pringle 1974; Milgrom 1976; Milgrom and Pines 1978; Parsignault *et al.* 1977), Cen X-3 (Schreier *et al.* 1976), and some other specific sources.

In this paper, we present the results of Monte Carlo calculations of X-ray light curves for binary systems surrounded by clouds with simple density distributions, chemical compositions, and ionization structures. Occultation of the X-radiation by the companion star, as well as Compton scattering and photoionization within the cloud, has been taken into account. The purpose of these simple models is to examine the effect of various cloud geometries and ionization structures upon the emergent X-ray flux as a function of orbital phase and X-ray energy. Our results are summarized in Figures 1 through 10. We have not attempted to construct a completely realistic model of the light curve of any specific X-ray binary; in particular, we have not considered the transfer of X-radiation through any accretion disk or other matter close to the X-ray star. Nonetheless, some of our results have direct application to the understanding of sources such as Cyg X-3 and Cen X-3, where transfer of the X-radiation through a cloud surrounding the binary system is evidently an important effect.

In § II of this paper, we describe the assumptions and method used to carry out our calculations. Our results are presented in § III, and the implications of these results for X-ray binary light curves in general and some specific sources in particular are discussed in § IV.

II. ASSUMPTIONS AND METHOD

We have constructed a simplified model of an X-ray source in a binary system surrounded by a scattering and absorbing medium. A compact star is assumed to be in a circular orbit about a normal stellar companion of radius R_s. The compact star emits X-rays isotropically, with random polarization, and with an

* This work was supported in part by the National Aeronautics and Space Administration under contract NAS5-11450.
† Alfred P. Sloan Research Fellow.

E^{-2} photon number spectrum. This arbitrary (but reasonable) spectrum is chosen because it is approximately invariant under Compton scattering in a cold electron gas (within the energy range of interest, $E \lesssim 20$ keV).

The density distribution of the gas cloud is assumed to be spherically symmetric with respect to the *companion* star and to have one of several simple radial density dependences. For each density distribution, we have used a Monte Carlo code to compute the X-ray light curve for (1) a range of values of R_s, (2) a range of Compton-scattering optical depths τ_e from the surface of the companion to infinity, and (3) various simple chemical compositions and ionization structures of the cloud. In all cases, the line joining the two stars of the binary system is a symmetry axis of the transfer problem.

We consider purely scattering clouds (complete ionization), as well as chemical compositions and ionization structures that entail photoelectric absorption. We do not, however, attempt to calculate self-consistent ionization structures for the cloud. The elements and ionization states are chosen to represent light, medium, and heavy ions at a variety of ionization temperatures. We use oxygen and iron to test the effects of medium-Z and high-Z elements, respectively. When absorption by iron is taken into account, its abundance by number relative to hydrogen is assumed to be $n_{\rm Fe}/n_{\rm H} = 3 \times 10^{-5}$; when absorption by both iron and oxygen are considered, we assume abundances of $n_{\rm Fe}/n_{\rm H} = 8 \times 10^{-6}$ and $n_{\rm O}/n_{\rm H} = 7 \times 10^{-4}$.

After a photon is emitted by the X-ray star, it undergoes Compton scattering until it is absorbed, reaches the surface of the companion star, or escapes from the system. In all cases, the X-ray albedo of the companion is assumed to be zero. (This simplifying assumption should have no qualitative effect upon our results, since any X-rays "reflected" by the companion would preferentially emerge near orbital phase 0.5 and would therefore have little effect upon the shape of the eclipse.) In the scattering events, the kinetic temperature of the electrons is assumed to be negligible and energy loss due to electron recoil is taken into account. The polarization of the photon is also taken into account for each scattering. In the case of absorption by iron, we incorporate the possibility that a fluorescent photon may be reemitted. However, we neglect all fluorescent photons from the cloud other than those that result from photoionizations by the photons in the Monte Carlo computations.

When a photon escapes the system, it is cataloged according to its direction and energy. The propagation of typically $\sim 10^5$ photons is computed for each X-ray light curve. Because of the symmetry axis in the system, each photon can be binned according to the angle ψ between its final propagation direction and the line joining the two stars; we choose the bins to have widths $\Delta\psi = 5°$. For this reason, our calculations result in fewer photons and hence have higher statistical fluctuations at orbital phases $\phi = 0$ and 0.5 than elsewhere. (We use the convention that $0 \leq \phi < 1$, with $\phi = 0$ corresponding to the center of the X-ray eclipse.) To reduce spurious features at these phases, we have smoothed the light curve by resetting the intensity I_n in any bin n near $\phi = 0$ or 0.5 according to

$$I_n = \tfrac{1}{2}(I_n' + I_0)\,,$$

where I_n' is the raw intensity measured for bin n and I_0 is the average intensity in several (two or three) adjacent bins. (All intensities discussed here and illustrated in the figures are in units of photons per unit solid angle per unit time.)

The X-ray light curves and spectra generated by these calculations are displayed for an observer in the orbital plane (orbital inclination angle $i = 90°$). Because of the aforementioned symmetry of the problem, light curves for $i < 90°$ can be constructed from our results by the simple transformation

$$\cos\phi' = \cos\phi/\sin i\,. \qquad (1)$$

Here, ϕ' is the true orbital phase at inclination i for which the X-ray intensity is identical to that at phase ϕ and $i = 90°$.

III. RESULTS

We have considered three models for the radial density distribution of the cloud. For two of the models, we have also considered several different simple ionization structures within the cloud. In each case, we first discuss the results for a completely ionized medium (i.e., pure Compton scattering with no photoelectric absorption). The model nomenclature is summarized in Table 1.

Model 1 is a uniform-density cloud with radius 4 times the binary orbital separation D. The results for pure Compton scattering in this model are shown in Figure 1. Two features are immediately apparent. (1) There is a nonzero X-ray intensity during the eclipse. This is a property of most of our models; photons that undergo their final scattering at points distant from the binary system, and are thus largely unocculted by the companion star, create an approximately isotropic flux. (2) The light curves tend toward a sinusoidal shape for large τ_e. This property is due to the asymmetry of the scattering cloud relative to the X-ray source. For large τ_e ($\gtrsim 5$), this is the primary influence on the shape of the light curve; the effect of the geometrical eclipse is fairly small (cf. Davidsen and Ostriker 1974).

TABLE 1

SUMMARY OF MODEL NOMENCLATURE

Model 1	Uniform-density cloud*
Model 2	Stellar wind* (density $\propto r^{-2}$)
Model 2a	Stellar wind with shadow
Model 2b	Stellar wind with Fe XXVI
Model 2c	Stellar wind with Fe and O
Model 3	Shell*
Model 3a	Shell with shadow
Model 3b	Shell with Fe and O

* Compton scattering only.

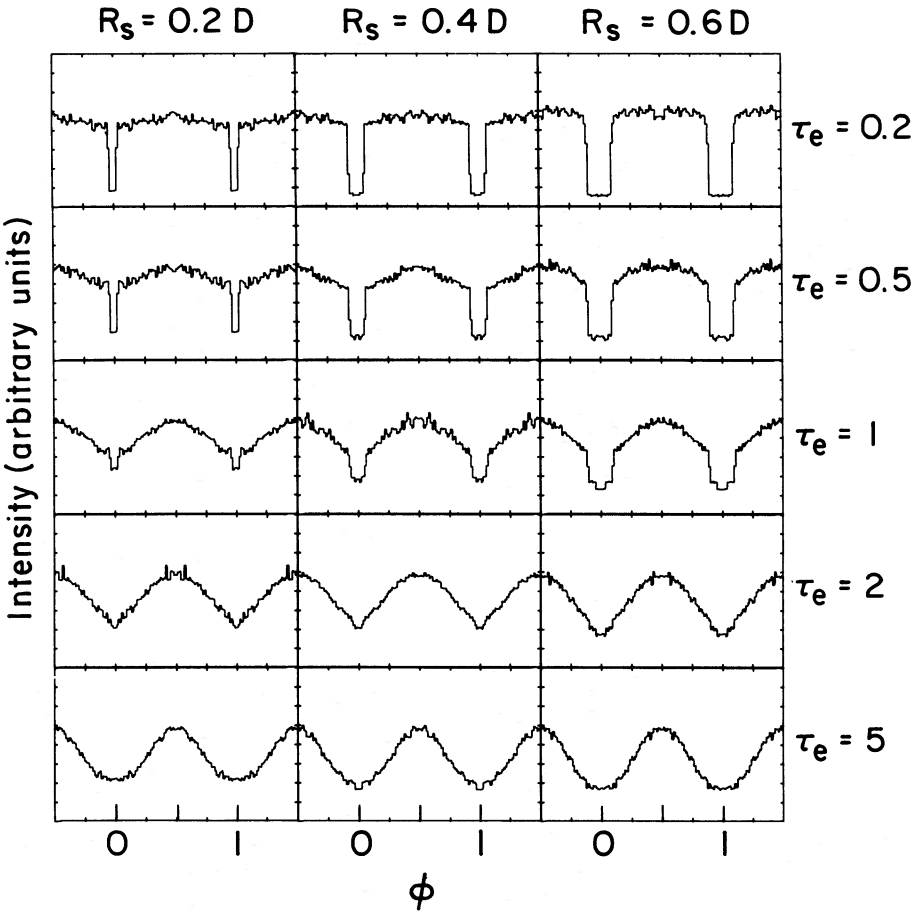

FIG. 1.—Simulated orbital X-ray light curves for model 1 (uniform-density cloud). The radius of the cloud is $4D$. Only the effects of Compton scattering from cold electrons are included in the computations. For each model, the radius of the stellar companion (R_s) and the Compton-scattering optical depth from the surface of the companion to infinity (τ_e) are indicated. The center of the X-ray eclipse is at orbital phase $\phi = 0$.

Model 2 is a steady-state, constant-velocity stellar wind emanating from the companion star. For this model, conservation of mass implies that the cloud will have an r^{-2} density dependence, where r is the distance from the center of the companion star. The resulting light curves for pure Compton scattering are shown in Figure 2. As τ_e increases, the optical depth from the X-ray star to the companion also increases and the probability for a photon to reach the companion star becomes small. Thus, for large values of τ_e, the shape of the light curve is determined entirely by the asymmetry of the cloud and becomes largely independent of R_s.

Model 3 is a spherically symmetric shell, or "cocoon," of the type proposed by Milgrom (1976) and Milgrom and Pines (1978) for Cyg X-3. In this model, the companion star is surrounded by a shell of matter with inner edge at $r_0 = 10D$ and with thickness $h = D$. (The resultant light curves are insensitive to r_0 and h, as long as $r_0 \gg D$ and $r_0 \gg h$.) The light curves for pure Compton scattering are shown in Figure 3. The shell is nearly symmetric with respect to the X-ray star, and the photons that scatter back into the cavity illuminate the shell approximately uniformly, so that the light curve tends to be much less modulated at large values of τ_e than in the previous cases (Figs. 1 and 2).

For models 2 and 3, we have also computed the light curves and observed spectra under the assumption that ionization is incomplete within part or all of the cloud. The results of these computations are described in the remainder of this section.

In model 2a, we assume that the matter is unionized and opaque to X-rays (absorption optical depth $\tau_a \gg 1$) in regions where the X-ray source is occulted by the companion star (i.e., in the "shadow" of the companion) and that ionization is complete everywhere else. (A more complete discussion of the degree of ionization in such a system is given by Hatchett and McCray 1977.) The resulting light curves are shown in Figure 4. The intensity minimum during eclipse is more pronounced than in the case of complete ionization (model 2, Fig. 2), since all photons that enter the "shadow" are assumed to be absorbed.

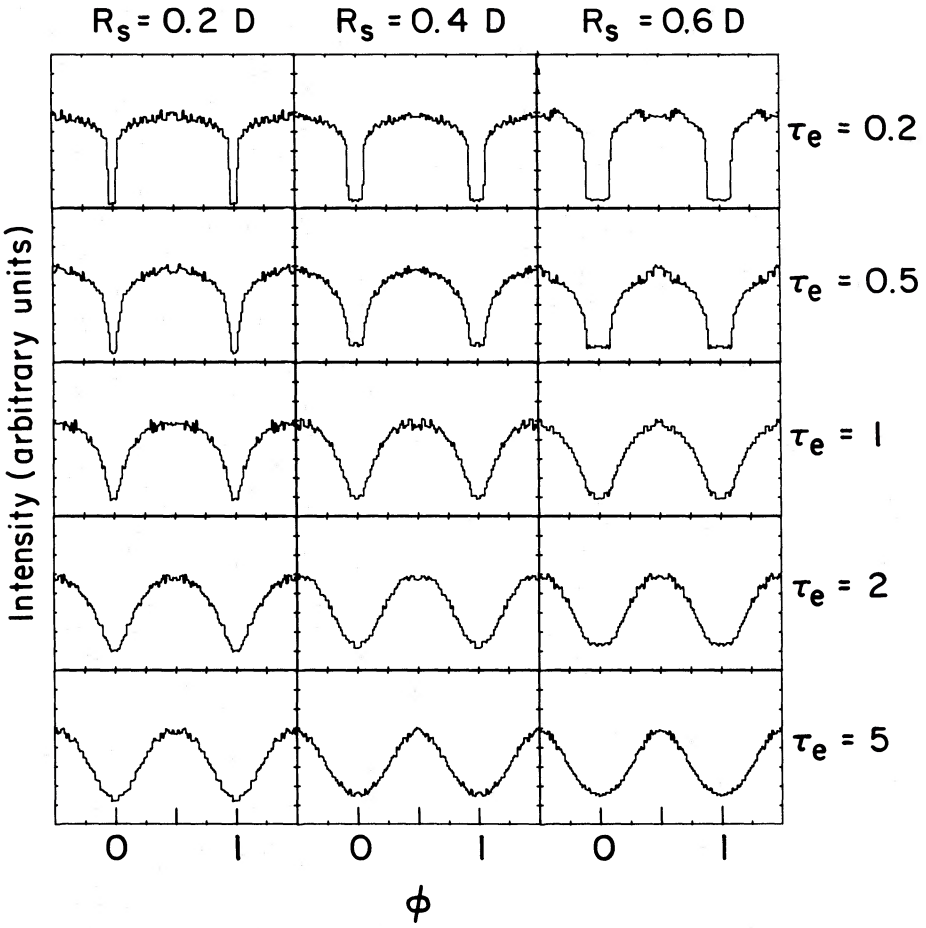

FIG. 2.—Simulated orbital X-ray light curves for model 2 (stellar wind). Only the effects of Compton scattering from cold electrons are included in the computations. The notation is the same as in Fig. 1.

In model 3a, we assume that the portion of the shell where the X-ray source is occulted by the companion star is again un-ionized and opaque to X-rays (i.e., completely absorbing). The resulting light curves are shown in Figure 5. Because of the absorption in the shadow of the companion, the light curves have appreciably deeper minima than for a purely scattering shell (model 3, Fig. 3), especially when $\tau_e \gtrsim 2$.

In model 2b, iron is assumed to be incompletely ionized and in the form of Fe XXVI throughout the cloud (including the shadow of the companion). This ionization structure roughly represents a cloud with a uniform ionization temperature $T \gtrsim 10^8$ K (see, e.g., Tucker and Koren 1971; Hatchett, Buff, and McCray 1976), at which lighter elements would be virtually completely ionized. In this ionization state, iron has a nearly 100% probability of producing a fluorescent X-ray for each photon absorbed (i.e., the collisional de-excitation rate is generally negligible). For simplicity, we assume that every recombination results in a Lα photon with energy 6.9 keV. Since no photons are lost to absorption, the resulting light curves are nearly identical (to within statistics) to those in model 2 (Fig. 2) at slightly larger values of τ_e. In Figure 6, we present the spectra for this model (with $R_s = 0.6D$) in three intervals of orbital phase. It is apparent that the equivalent widths of the iron absorption/emission features are slightly enhanced in the orbital phase range $\phi = 0.75$–1.0 over those in the $\phi = 0.5$–0.625 range; this effect results from a larger mean number of scattering events per photon in the $\phi = 0.75$–1.0 range. However, the variation in equivalent width is less pronounced for $\tau_e \gtrsim 2$, because the great majority of photons with energies just above the absorption edge of Fe XXVI at 9.2 keV are absorbed, regardless of their direction of propagation. In general, we find that the strengths of the spectral features do not vary greatly with orbital phase.

In model 2c, we assume that both oxygen and iron are present and in a state of low ionization (as might be expected in a cloud with $T \lesssim 3 \times 10^5$ K throughout [see, e.g., Hatchett, Buff, and McCray 1976]). We assume that all of the iron has a fluorescent yield of 0.3, which is appropriate to iron in a low ionization state (Bambynek *et al.* 1972). In Figure 7, we present the resultant light curves in three different energy

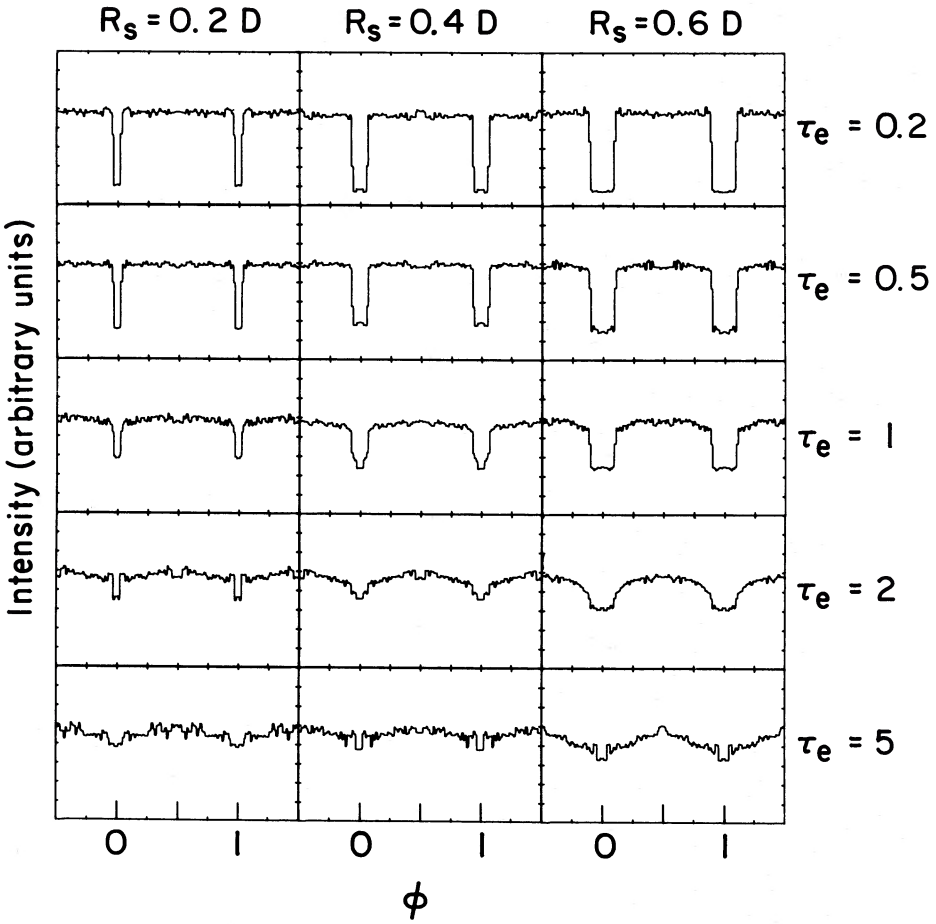

FIG. 3.—Simulated orbital X-ray light curves for model 3 (shell). The radius of the shell is $10D$. Only the effects of Compton scattering from cold electrons are included in the computations. The notation is the same as in Fig. 1.

bands for $R_s = 0.6D$. The absorption of low-energy photons by oxygen is very evident. For $\tau_e \gtrsim 2$, almost no photons below 3 keV escape from the system. For the low- and medium-energy light curves, the absorption is most pronounced near the edges of the X-ray eclipse. A comparison of the high-energy light curves with the light curves of model 2 (Fig. 2) indicates little difference, as expected. In Figure 8, we show the spectra for this model in three intervals of orbital phase. It is again apparent that, aside from the total intensity, the spectrum depends only weakly on orbital phase.

In model 3b, we include absorption by un-ionized oxygen and iron throughout the shell that surrounds the system. (We do *not* assume that the portion of the shell in the shadow of the companion star is opaque to X-rays.) This model is similar to the model for Cyg X-3 that was proposed by Milgrom (1976) and Milgrom and Pines (1978), except that we do not use a self-consistent ionization structure for the shell (see § IV). The resultant light curves for $R_s = 0.6D$ are shown in Figure 9. When the optical depth is sufficiently large for the light curves to have a roughly sinusoidal shape ($\tau_e \gtrsim 2$), the modulation of the light curves is larger than for a purely scattering shell (model 3, Fig. 3) and is comparable to that obtained for a shell with an opaque cap in the shadow of the companion star (model 3a, Fig. 5). The spectra as a function of orbital phase for this model (Fig. 10) are not greatly different from those obtained for model 2c (Fig. 8), which indicates that the spectrum does not depend sensitively upon the details of the cloud geometry.

IV. DISCUSSION

We have computed the X-ray light curves as a function of energy for X-ray sources in binary stellar systems surrounded by clouds with a variety of geometries and ionization structures. Our results, presented in Figures 1–10 (see also Table 1), demonstrate the sensitivity of the observed light curve and orbital-phase–dependent spectrum upon the optical depth, geometry, and ionization structure of such a cloud. We caution that these models do not take into account all of the complexities in the transfer of

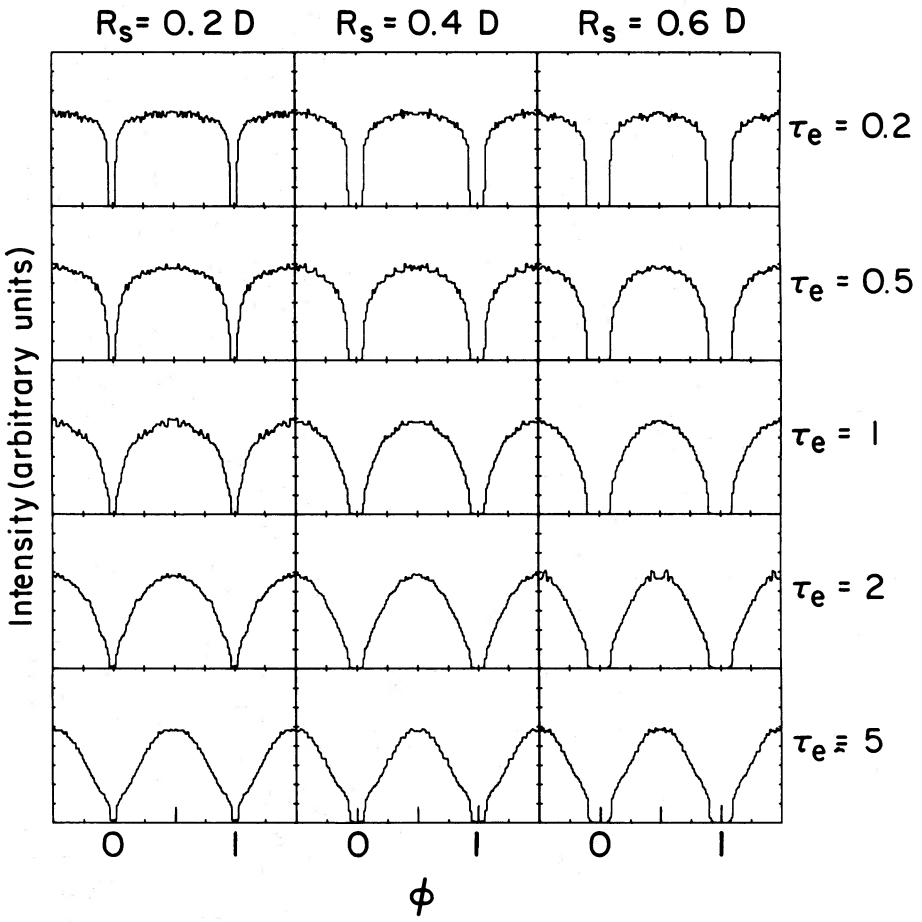

FIG. 4.—Simulated orbital X-ray light curves for model 2a (stellar wind with shadow). The effects of Compton scattering from cold electrons, as well as photoelectric absorption within the shadow of the companion star, are included in the computations (see text). The notation is the same as in Fig. 1.

X-radiation through a real X-ray binary system. In particular, we emphasize that the cloud chemical compositions and ionization structures that we have chosen are highly simplified. However, we find that the X-ray light curve and orbital-phase–dependent spectrum are not highly sensitive to the details of the density structure or ionization structure in such a cloud.

The properties of Cen X-3 (Schreier *et al.* 1976) and several other X-ray binaries have been interpreted in terms of a strong stellar wind that emanates from the companion star. Schreier *et al.* (1976) discussed variations in the light curve and phase-dependent spectrum of Cen X-3 in terms of variations in the X-ray optical depth of the stellar wind; the dependence on τ_e of the energy-dependent light curves and phase-dependent spectra for model 2c (Figs. 7 and 8) is in good qualitative agreement with their discussion. We note, however, that the variations in the light curve with τ_e in our model are due entirely to variations in the density of the stellar wind, whereas a variable ionization structure surrounding the X-ray star is a central component of the picture envisaged by Schreier *et al.* (1976).

The observed nonzero eclipse intensity of Cen X-3 (Schreier *et al.* 1976) is adequately fitted by model 1 or 2 (Figs. 1 and 2) with $\tau_e \approx 0.2$ and $R_s \approx 0.6D$. For the Cen X-3 system, we have $R_s \approx 10^{12}$ cm (Krzeminski 1974); in model 2, this corresponds to an electron density of $\sim 10^{11}$ cm^{-3} at the orbit of the neutron star, in good agreement with the value predicted by Davidson and Ostriker (1973) on the basis of the observed accretion-driven X-ray luminosity.

As noted above, Milgrom (1976) and Milgrom and Pines (1978) have proposed a model for the X-ray light curve of Cyg X-3 that relies on X-ray transfer through a cocoon of matter that surrounds the binary system. The essential features of the observed X-ray light curves are (1) an approximately sinusoidal shape (but with a slightly broader maximum and narrower minimum than for a simple sinusoid), (2) a substantial but not extremely large intensity modulation (ratio of maximum to minimum X-ray intensity ~2–3), (3) a spectral feature consistent with iron-line emission,

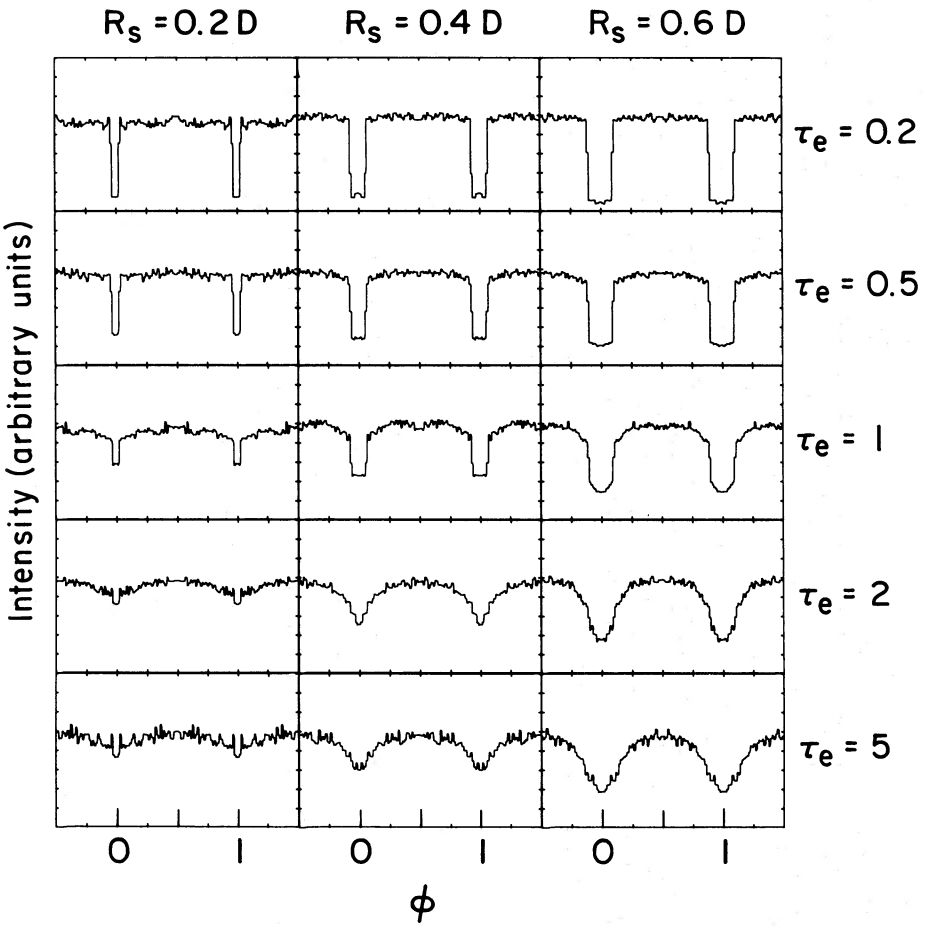

FIG. 5.—Simulated orbital X-ray light curves for model 3a (shell with shadow). The effects of Compton scattering from cold electrons, as well as photoelectric absorption within the shadow of the companion star, are included in the computations (see text). The notation is the same as in Fig. 1.

visible at all orbital phases, and (4) no discernible spectral variability with orbital phase. (These observations are reported by Parsignault *et al.* 1972; Sanford and Hawkins 1972; Canizares *et al.* 1973; Leach *et al.* 1975; Sanford, Mason, and Ives 1975; Serlemitsos *et al.* 1975; Ulmer 1975; Mason *et al.* 1976; Parsignault *et al.* 1977.)

As pointed out by Parsignault *et al.* (1977), the strengths of the observed spectral features strongly suggest that the X-ray transfer medium cannot be highly underabundant in heavy elements, and the apparent constancy of the spectrum with orbital phase then tends to rule against a constant-velocity stellar wind as the medium (cf. Davidsen and Ostriker 1974; Pringle 1974). A careful comparison of the phase-dependent spectra for models 2c and 3b (Figs. 8 and 10, respectively) provides further evidence for this conclusion. The models that reasonably reproduce the X-ray light curve of Cyg X-3 have electron-scattering optical depths of $\tau_e \gtrsim 2$, and for these models the low-energy cutoff of the X-ray spectrum is more nearly independent of orbital phase when the X-ray transfer medium is a shell rather than a constant-velocity wind. Moreover, the shape of the light curve is more nearly independent of X-ray energy for the shell (Fig. 9) than for the constant-velocity wind (Fig. 7). (The increased eclipse depth at lower X-ray energies in both of these models [Figs. 7 and 9] results from the increased absorption optical depth near $\phi = 0$.)

A comparison of the X-ray light curves for the shell models 3, 3a, and 3b (Figs. 3, 5, and 9, respectively) indicates that a shape and modulation comparable to those of the Cyg X-3 light curve are obtained only if $\tau_e \gtrsim 2$, $R_s \gtrsim 0.6D$, and photoelectric absorption occurs within part or all of the shell (cf. Milgrom 1976). The self-consistent ionization structure of Milgrom's (1976) cocoon model is intermediate between model 3a (absorption only in the X-ray shadow of the companion star) and model 3b (photoelectric absorption throughout the shell). In fact, among the models that we have studied, these are the two that most nearly replicate the light curve of Cyg X-3.

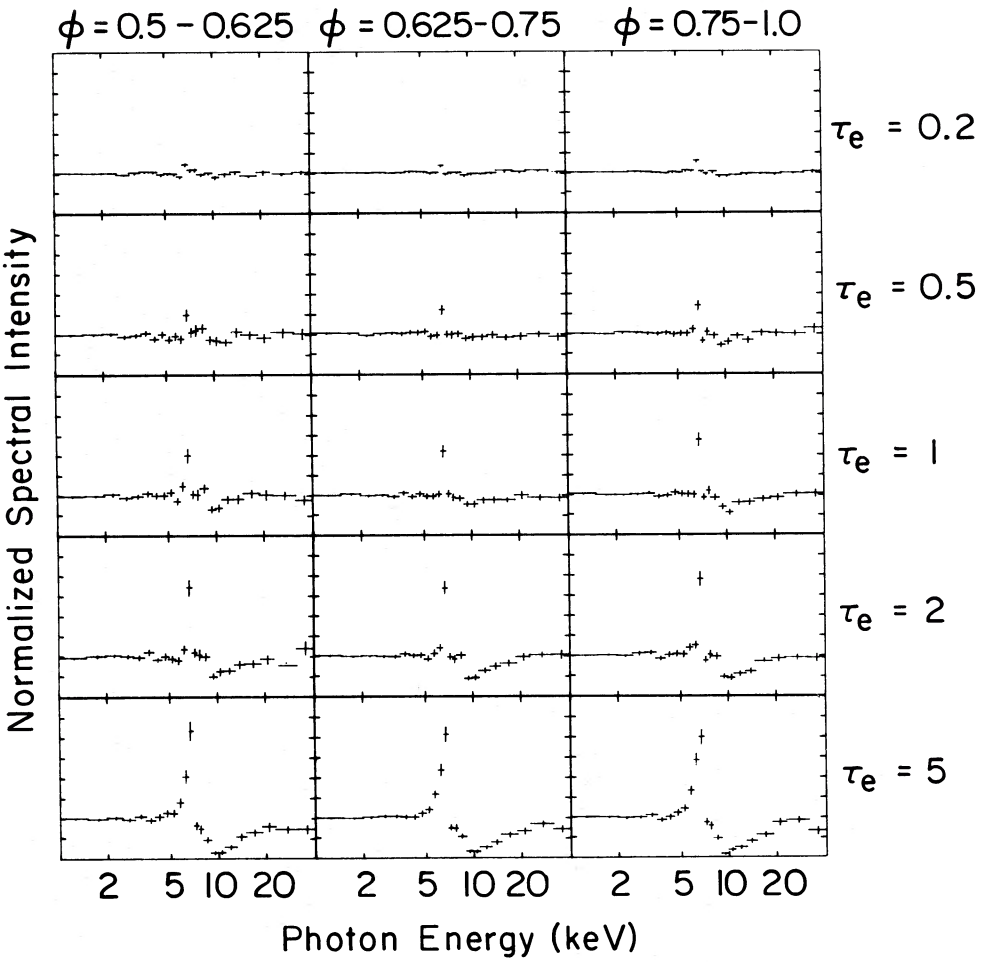

FIG. 6.—Simulated X-ray spectra for model 2b (stellar wind with Fe XXVI) with $R_s = 0.6D$, as a function of orbital phase. In each case, the spectrum is averaged over the indicated range of orbital phase and normalized to the source spectrum. The horizontal bars denote the sizes of the spectral bins, and the vertical bars denote 1 σ statistical uncertainties. The effects of Compton scattering, as well as photoelectric absorption and fluorescent reemission by Fe XXVI, are included in the computations (see text).

In view of the encouraging level of agreement between the basic picture envisaged by Milgrom (1976) and the numerical results of our Monte Carlo calculations for models 3a and 3b, we have investigated some of the properties of these models in more detail. We reach the following conclusions (cf. Milgrom 1976): (1) For $\tau_e \lesssim 2$, photons that pass directly through the shell without interaction contribute noticeably to the total light curve; (2) for $\tau_e \gtrsim 2$, a photon entering the shell has a higher probability of being scattered back into the intrashell cavity than of escaping the system; and (3) the intensity per unit solid angle of scattered photons emerging from the outer surface of the shell is very nearly proportional to $\cos\gamma$, where γ is the angle to the normal from the shell surface. We also note that this model for the X-ray light curve of Cyg X-3 is at best incomplete, since it is unclear whether the requisite shell of matter could be stable (cf. Parsignault *et al.* 1977; Milgrom and Pines 1978). However, as suggested by Milgrom (1976), the large distance of most of the scattering and absorbing matter from the binary stellar orbit may well be the only essential geometrical feature of this simple model. As a test of this hypothesis, we have calculated the X-ray light curve for a fully ionized uniform-density cloud with radius $10D$, $R_s = 0.6D$, and $\tau_e = 2$. We find that this light curve is very similar to the equivalent light curve for a fully ionized shell of radius $10D$ (Fig. 3), which tends to confirm Milgrom's (1976) assertion.

Our calculations provide some insight into the problem of the lack of observed eclipses in the X-ray sources that appear to be associated with the galactic bulge. Many of these sources—including several X-ray burst sources, the bright galactic-center sources, and several globular-cluster sources—have been observed sufficiently well to rule out the presence of eclipses or other substantial periodic modulation of the X-ray intensity on orbital time scales (Joss and Rappaport 1978). There are at least four possible explanations

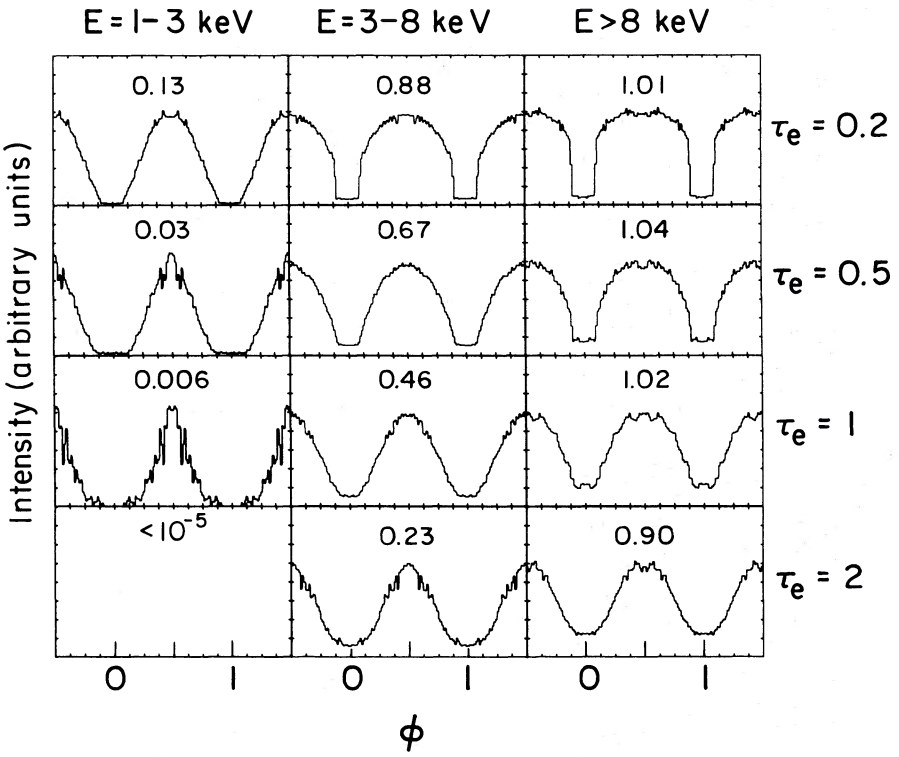

FIG. 7.—Simulated orbital light curves as a function of X-ray energy for model 2c (stellar wind with O and Fe) with $R_s = 0.6D$. Compton scattering within the cloud, photoelectric absorption by un-ionized oxygen and iron, and fluorescent reemission by iron are taken into account in the computations (see text). The number above each light curve is the ratio of the maximum intensity of the light curve to the intensity emitted isotropically by the X-ray source. The notation is otherwise the same as in Fig. 1. Light curves for $\tau_e = 5$ were not generated because of the excessive computation times required.

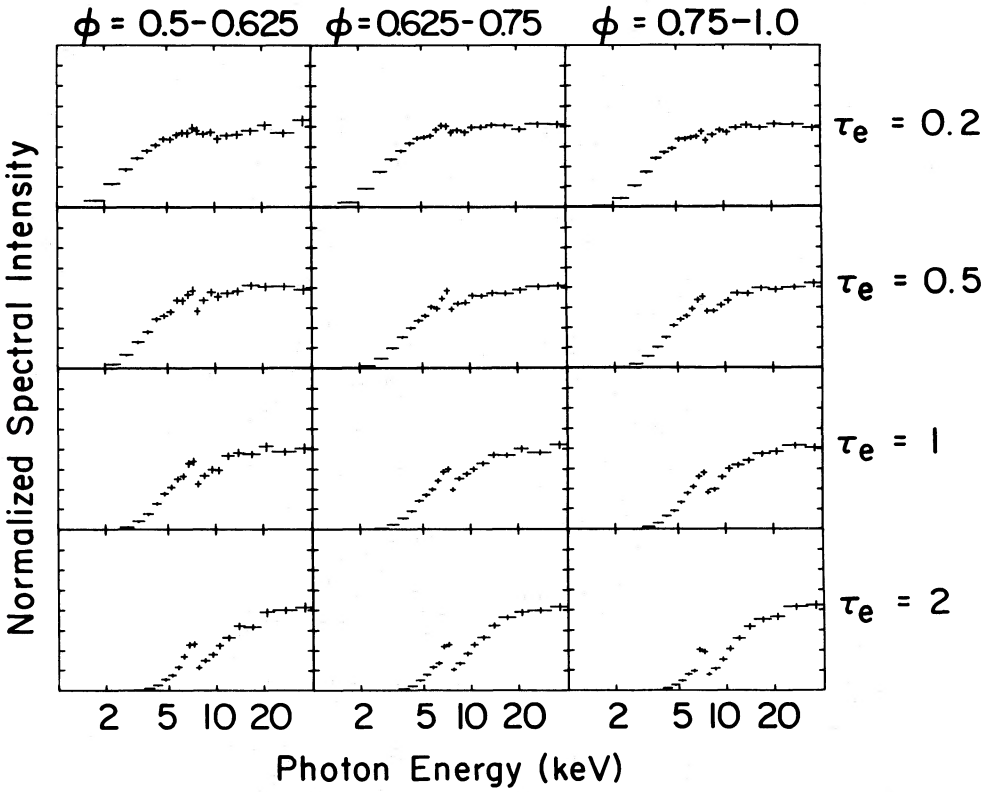

FIG. 8.—Simulated X-ray spectra for model 2c (stellar wind with O and Fe) with $R_s = 0.6D$, as a function of orbital phase. In each case, the spectrum is averaged over the indicated range of orbital phase and normalized to the source spectrum. The horizontal bars denote the widths of the spectral bins, and the vertical bars denote 1 σ statistical uncertainties. The effects of Compton scattering, photoelectric absorption by un-ionized oxygen and iron, and fluorescent reemission by iron are included in the computations (see text).

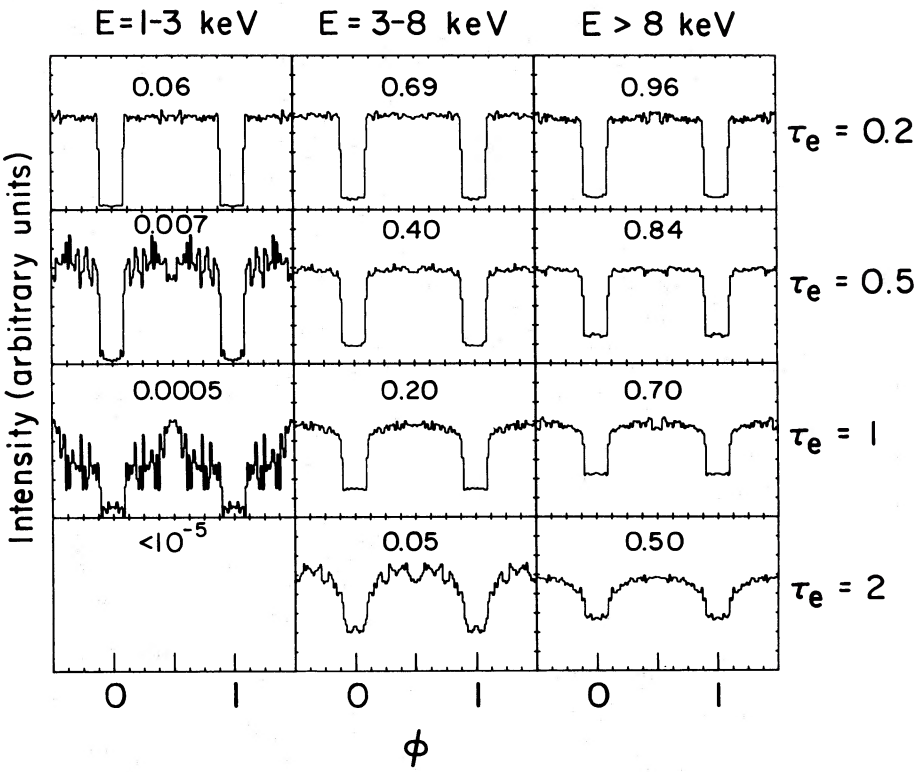

FIG. 9.—Simulated orbital light curves as a function of X-ray energy for model 3b (shell with O and Fe) with $R_s = 0.6D$. Compton scattering within the cloud, photoelectric absorption by un-ionized oxygen and iron, and fluorescent reemission by iron are taken into account in the computations (see text). The number above each light curve is the ratio of the maximum intensity of the light curve to the intensity emitted isotropically by the X-ray source. The notation is otherwise the same as in Fig. 1. Light curves for $\tau_e = 5$ were not generated because of the excessive computation times required.

for these observations: (1) The sources are not in binary systems; (2) the sources are in binary systems that have very wide orbits, wherein the companion stars greatly underfill their critical potential lobes; (3) the binary stellar companions of the X-ray sources are of low mass and have small critical lobes; or (4) the X-ray binary systems are surrounded by obscuring clouds. Hypothesis (1) is difficult to disprove, although there is no direct evidence to support it. With hypothesis (2), it is difficult to understand how efficient mass transfer could be achieved for wide stellar separations. Moreover, there is no optical evidence that any of these sources have massive companions with strong stellar winds. Hypothesis (3) is explored in depth by Joss and Rappaport (1978), who conclude that it is tenable for many, if not all, of these sources.

On the basis of the calculated X-ray light curves for the models that we have studied in the present work, we conclude that hypothesis (4) is unlikely. For $R_s \gtrsim 0.4D$ and a cloud with a scale size comparable to the binary separation, the X-ray eclipses apparently cannot be obscured unless (*a*) τ_e is substantially larger than 5 and (*b*) the cloud has either an anomalously low heavy-element abundance ($\lesssim 10^{-4}$ by mass) or an extremely high level of ionization. If condition (*b*) is not satisfied, the low-energy cutoffs due to photoelectric absorption will be substantially larger than the ~ 2 keV cutoffs that are typical of the galactic-bulge sources (Jones 1977). In the case of clouds that are very large or have shell-like structures, X-ray eclipses can be masked for τ_e as small as ~ 5. For Population II systems with very low heavy-element abundances, the resultant low-energy cutoffs might then be consistent with the observations. However, the existence of this type of cloud may require the presence of an active young pulsar as the collapsed star (cf. the discussions of Cyg X-3 by Milgrom and Pines 1978 and references therein).

We are grateful to R. McCray, M. Milgrom, and D. Parsignault for stimulating discussions.

Note added in manuscript, 1977 March.—Becker *et al.* (1978) have recently reported the detection with *OSO 8* of weak X-ray emission from 4U 0900−40 during the X-ray eclipses of that source. We point out that this emission is similar to that observed in Cen X-3 (Schreier *et al.* 1976) and that the effect can be understood in terms of our models for X-ray transfer through a binary system (see § IV).

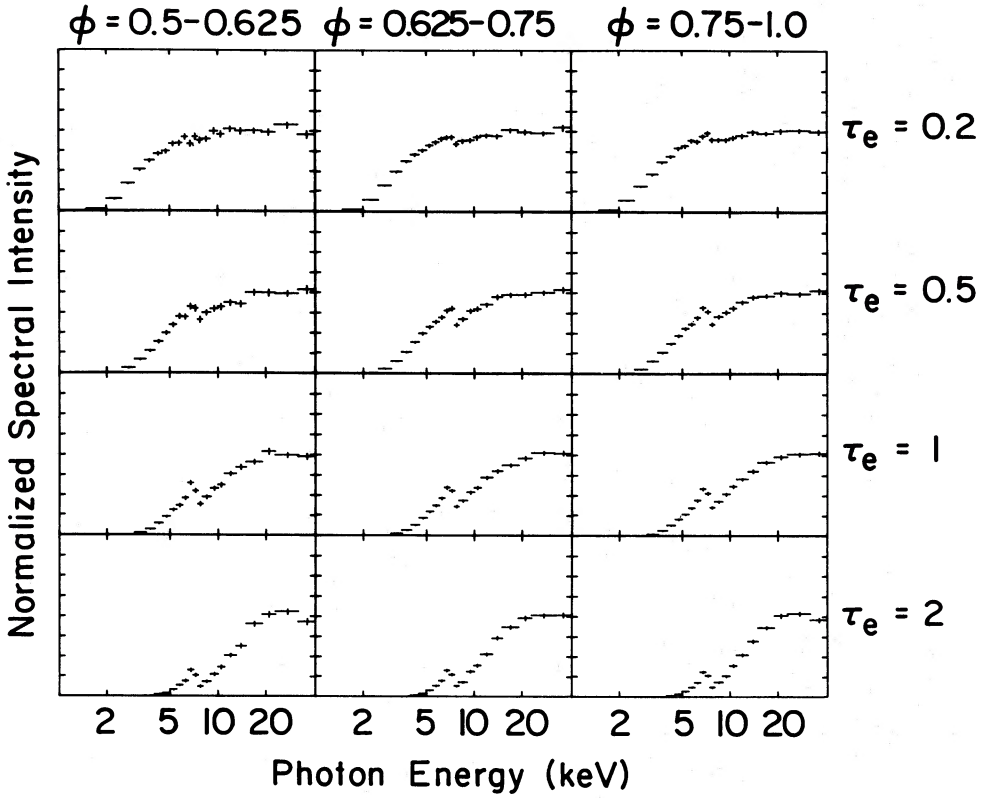

FIG. 10.—Simulated X-ray spectra for model 3b (shell with O and Fe) with $R_s = 0.6D$, as a function of orbital phase. In each case, the spectrum is averaged over the indicated range of orbital phase and normalized to the source spectrum. The horizontal bars denote the sizes of the spectral bins, and the vertical bars denote 1 σ statistical uncertainties. The effects of Compton scattering, photoelectric absorption by un-ionized oxygen and iron, and fluorescent reemission by iron are included in the computations (see text).

REFERENCES

Bambynek, W., *et al.* 1972, *Rev. Mod. Phys.*, **44**, 716.
Becker, R. H., Rothschild, R. E., Boldt, E. A., Holt, S. S., Pravdo, S. S., Serlemitsos, P. J., and Swank, J. H. 1978, preprint.
Buff, J. S., and McCray, R. 1974*a*, *Ap. J.* (*Letters*), **188**, L37.
———. 1974*b*, *Ap. J.*, **189**, 147.
Canizares, C. R., McClintock, J. E., Clark, G. W., Lewin, W. H. G., Schnopper, H. W., and Sprott, G. F. 1973, *Nature Phys. Sci.*, **241**, 28.
Davidsen, A., and Ostriker, J. P. 1974, *Ap. J.*, **189**, 331.
Davidson, K., and Ostriker, J. P. 1973, *Ap. J.*, **179**, 585.
Hatchett, S., Buff, J., and McCray, R. 1976, *Ap. J.*, **206**, 847.
Hatchett, S., and McCray, R. 1977, *Ap. J.*, **211**, 552.
Jones, C. 1977, *Ap. J.*, **214**, 856.
Joss, P. C., and Rappaport, S. 1978, *Astr. Ap.*, in press.
Krzeminski, W. 1974, *Ap. J.* (*Letters*), **192**, L135.
Leach, R. W., Murray, S. S., Schreier, E. J., Tananbaum, H. D., Ulmer, M. P., and Parsignault, D. R. 1975, *Ap. J.*, **199**, 184.
Mason, K. O., *et al.* 1976, *Ap. J.*, **207**, 78.
Milgrom, M. 1976, *Astr. Ap.*, **51**, 215.
Milgrom, M., and Pines, D. 1978, *Ap. J.*, **220**, 272.
Parsignault, D. R., Grindlay, J., Gursky, H., and Tucker, W. 1977, *Ap. J.*, **218**, 232.
Parsignault, D. R., *et al.* 1972, *Nature Phys. Sci.*, **239**, 123.
Pringle, J. E. 1973, *Nature Phys. Sci.*, **243**, 90.
———. 1974, *Nature*, **247**, 21.
Sanford, P. W., and Hawkins, F. M. 1972, *Nature Phys. Sci.*, **239**, 135.
Sanford, P. W., Mason, K. O., and Ives, J. 1975, *M.N.R.A.S.*, **173**, 9P.
Schreier, E. J., Swartz, K., Giacconi, R., Fabbiano, G., and Morin, J. 1976, *Ap. J.*, **204**, 539.
Serlemitsos, P. J., Boldt, E. A., Holt, S. S., Rothschild, R. E., and Saba, J. L. R. 1975, *Ap. J.* (*Letters*), **201**, L9.
Tarter, C. B., and Salpeter, E. E. 1969, *Ap. J.*, **156**, 953.
Tarter, C. B., Tucker, W. H., and Salpeter, E. E. 1969, *Ap. J.*, **156**, 943.
Tucker, W. H., and Koren, M. 1971, *Ap. J.*, **168**, 283.
Ulmer, M. P. 1975, *Ap. J.*, **196**, 827.

PAUL HERTZ: Harvard University, Center for Astrophysics, 60 Garden Street, Cambridge, MA 02138

PAUL C. JOSS and SAUL RAPPAPORT: Room 6-203, Massachusetts Institute of Technology, Cambridge, MA 02139